Nuclear Instruments and Methods in Physics Research A 699 (2013) 198–204

Contents lists available at SciVerse ScienceDirect

Nuclear Instruments and Methods in Physics Research A

journal homepage: www.elsevier.com/locate/nima

Measuring radiation environment in LHC or anywhere else, on your computer screen with Medipix

Erik H.M. Heijne [a,c,*], Rafael Ballabriga Sune [a], Michael Campbell [a], Claude Leroy [b], Xavier Llopart [a], Jean-Pierre Martin [b], Stanislav Pospisil [c], Jaroslav Solc [c], Paul Soueid [b], Michal Suk [c], Lukas Tlustos [a], Daniel Turecek [c], Zdenek Vykydal [c], Winnie Wong [a]

[a] CERN, CH1211 Geneva23, Switzerland
[b] Université de Montréal, Canada
[c] Institute of Experimental and Applied Physics, Czech Technical University in Prague, Czech Republic

with ATLAS-MPX collaboration and Medipix Collaboration

ARTICLE INFO

Available online 29 May 2012

Keywords:
Quantum dosimetry
Dose rate
Pixel detector
Particle detector
Background radiation

ABSTRACT

The Medipix family of chips use on-pixel pulse processing front-ends, digitization and counters to produce images of radiation. The devices have been derived from developments for the Large Hadron Collider (LHC) physics experiments at CERN. With the miniaturization of the associated readout system a new method of dosimetry becomes accessible, where single radiation quanta are detected and imaged. Several examples of dose measurements at highly differing dose rates are presented here: monitoring of background radiation on earth, in a flying airplane and in the ATLAS experiment at LHC. During proton collision runs as well as during the stops of the accelerator the dose can be measured, including characterization of different types of radiation. Thanks to the noiseless method of quantum imaging dosimetry, a large dynamic range can be achieved, employing only this single device. The dose rate extends from recording only a few quanta in hours, up to hundreds of quanta recorded in a fraction of a ms. With complementary methods for the analysis of the exposed image frames, one can cover 14 orders of magnitude.

1. Introduction

The development of pixel imagers for elementary particles based on CMOS microelectronics has resulted in a key technology for the LHC physics experiments [1,2]. It is very well possible to exploit this also for the measurement of various radiation fields, even at very low intensity, such as for sea-level cosmics or the natural background. Using the characteristic clusters resulting from interaction of different types of radiation one can determine the components of the radiation field in real time [3,4]. In Sections 2 and 3 the basic characteristics of the family of Medipix imaging pixel detectors are briefly described and the connection between this 'quantum imaging dosimetry' and usual dose units is discussed. We emphasize the dynamic range $>10^{14}$ obtained with a single device. As a first example, in Section 4 measurements are shown that were made in ATLAS using 16 specially adapted Medipix2 devices in different positions. Fig. 1 shows a photograph of a complete system of Medipix2 assembly and USB readout box [5]. Further miniaturization has resulted in a radiation imaging monitor in the form of a USB memory stick, that easily can be used everywhere, as shown later. Measurements in-flight of cosmic rays at high altitude illustrate this possibility in Section 5. While in these first applications the Medipix2 chip with a 'binary' image was used, just counting 'hit/no-hit', in the more advanced Timepix device it is possible to determine also the amount of energy deposited in each pixel. This helps to improve the cluster characterization, and at the same time it provides a measure of the total energy deposited in the full sensor, during the exposure. Contrary to the new quantum cluster count, this quantity can be more easily compared with the traditional dose measurements. An example is discussed in Section 6.

2. Dosimetry with large dynamic range using imaging of radiation quanta with Medipix

The Medipix readout chips are in most cases connected via microscopic bump contacts to a matched, thin (0.3 mm) silicon sensor [6]. Other semiconductor sensor materials, gaseous detectors or microchannel plates may be used as well. While in all devices the

* Corresponding author at: CERN PH Department, CH1211 Geneva23, Switzerland.
E-mail address: erik.heijne@cern.ch (E.H.M. Heijne).

0168-9002/$ - see front matter © 2012 Elsevier B.V. All rights reserved.
http://dx.doi.org/10.1016/j.nima.2012.05.023

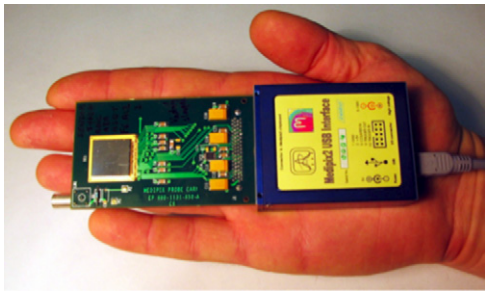

Fig. 1. The Medipix2 assembly mounted on a printed circuit board (PCB) and connected to the USB readout box. The reverse bias voltage for the pixel sensor is supplied through the Lemo™ connector at the bottom left. All other connections are made through the connector between the PCB and the USB box. The USB box is directly connected to a USB port on a (portable) computer, and all can be controlled by Pixelman™ software on this computer.

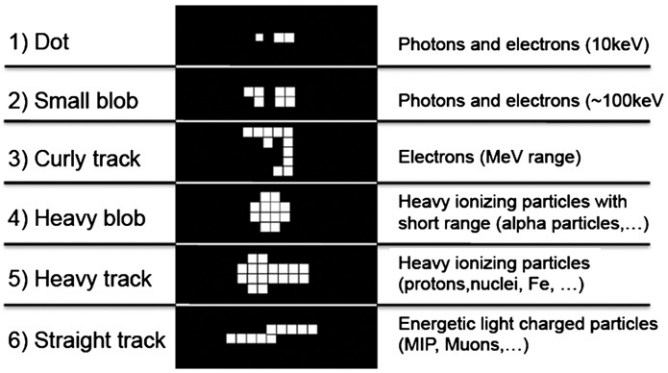

Fig. 2. Characteristic patterns of clusters that are created by incident radiation quanta in the Medipix pixel matrix (from [4]). In a first approximation one can distinguish the 6 illustrated patterns. At the right are enumerated the types of particles to which these patterns can be attributed. A perpendicular incident muon or MIP also results in a 'dot' pattern. It can be recognized by its higher signal. Laterally the pixel is 55 μm but perpendicularly it is 300 μm of Si.

55 μm square pixels are arranged in a 256×256 matrix, the capabilities of the readout chip have evolved over time and more advanced versions have been introduced. The original Medipix1 [7] has been followed so far by Medipix2 [6], Timepix [8] and Medipix3 [9]. In all designs a signal processing chain with logic is accommodated in each pixel, which can function as an independent detection element. The full pixel matrix can be switched to active exposure or can be frozen by a common shutter signal that is distributed all over the 14 mm × 14 mm area within some ns. When during the exposure time a certain amount of energy is deposited in a sensor pixel by a radiation quantum and the resulting signal exceeds the pre-set threshold value, the pixel hit counter is incremented. The energy threshold in each pixel for the registration of a hit can be set typically as low as ~4 keV and images can be obtained with a ^{55}Fe radioactive source, that emits 5.9 keV X-photon quanta. The fairly linear threshold curve can be calibrated electronically, or using e.g. a ^{241}Am source (26.3 and 59.5 keV gamma + several X-rays from Np). All pixel counter values are read out sequentially after termination of the exposure, and then reset to zero. When the device is used for imaging in an intense X-ray flux, each pixel can be hit many times and the pixel records the intensity in the 14-bit register. With the signal shaping time of ~1 μs a continuous random hit rate close to 1 MHz per pixel is possible without appreciable deadtime. However, in most dosimetry applications the intensity is many orders of magnitude lower and the individual incoming quanta produce just one count in the pixel(s) that they hit. These sparse pixel hits remain separated in the matrix by large areas of zero-hit pixels. The quanta produce characteristic hit patterns as illustrated in Fig. 2 and earlier discussed in [3,4].

Only when two independent clusters have some overlap, there are a few pixels with two counts. Automatic cluster recognition can be used as long as the number of overlapping clusters is small. In order to achieve the optimal cluster density of ~100 per frame, the exposure time can be adjusted over a very large range. A minimum exposure time of 10 μs for the complete matrix is possible with ~10 ns precision of the electronic shutter, and a maximum single exposure time can be well over one day (e.g. 30 h is 1.08×10^{11} μs). This precise, variable exposure time is the main component for the large dynamic range, and already 10^{10} is provided by this mechanism alone. A typical factor of 15 comes from the range of acceptable cluster densities between 10 and 150. Finally, when the radiation intensity is too high for cluster recognition, even at very short exposures, one can still count the total number of hits that have been registered in all pixels. Each of the 65,000 pixels has a 14-bit register, so that in principle any integral sum of counts between zero and $\sim 8 \times 10^8$ could be realized. Possible overflow of pixels under high rates and statistical distributions in practice lead to a limit of order 10^5. Still, this adds a large factor to the dynamic range. All together, one can cover a dynamic range of at least 10^{14} with a single device. Contrary to the situation for many other types of imagers, there is hardly any noise in the Medipix images when the signal comparator thresholds are properly tuned. An occasional bad pixel can be switched off, generally fewer than 10 for the 65,000 pixels.

3. Quantitative analysis and quality factor

Rigorous details of equivalent dose determination, including radiation weighting factors are beyond the scope of this paper, which aims only to describe some examples. The absorbed dose (Gy/kg) is not very different in Si or in body tissue. The Linear Energy Transfer LET is ~0.4 keV/μm in Si for typical ionizing particles such as electrons or muons but it can be higher, such as for low energy protons. The energy deposit in a 55 μm pixel, if the particle 'wanders' through the Si sensor is typically ~20 keV, and the deposit can be much higher if the particle travels perpendicular through the 300 μm thick sensor. In body tissue of smaller density the LET is about half this value. Usually, most of the incident radiation consists of photons and electrons, which have a radiation weighting factor (former quality factor) of 1 for conversion from absorbed dose (Gy) into equivalent dose H_T (Sv) for an organ T. In the examples, the absorbed dose in Si is not converted to a tissue value, but in some cases the influence of a quality factor is discussed.

Photons can be detected only after they create a secondary electron. An estimate of the photon/electron energy deposit can be made using the length of the ionization trail that the electron leaves in the sensor. For calibration a Medipix2 Si hybrid assembly has been exposed to photons from a ^{60}Co source and from a ^{137}Cs source, as illustrated in the Fig. 3a and b. These were standard sources and allowed to determine the conversion factor between the calibrated air kerma and the number of clusters, as indicated in the captions. The average value of 2.0×10^{-10} Sv per visible cluster is a reasonable first approximation.

Cluster analysis and pattern recognition allow one to distinguish typical radiation quanta that have a quality factor >1. These can be alpha particles from radioactive decay, alphas from neutron conversions or heavily ionizing particles such as low energy protons or ionized nuclei. Some examples will be encountered later on. Quality factors can be applied on these classes of clusters in order to ultimately determine the effective dose.

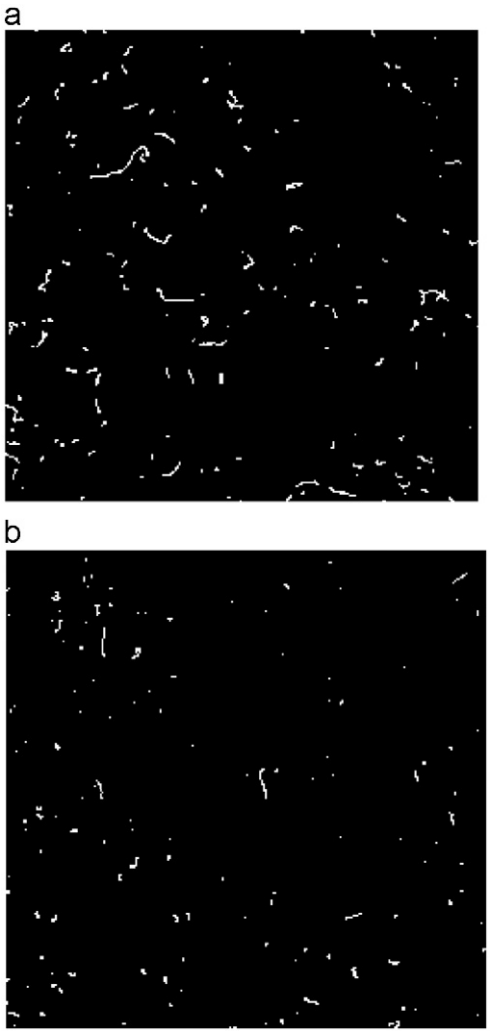

Fig. 3. (a)Exposure to a ^{60}Co source with photon energy 1173 and 1333 keV; $2.3 \pm 0.2 \times 10^{-10}$ Sv per cluster. (b) Exposure to a ^{137}Cs source with photon energy 662 keV; $1.7 \pm 0.1 \times 10^{-10}$ Sv per cluster.

Using a Medipix2 device the dose has been determined with two different methods:• **cluster counting**: assign 2×10^{-10} Sv per visible cluster for electrons and $Q \times 2 \times 10^{-10}$ Sv per cluster of heavy particles: 1 Sv=1 Gy x quality Q=1 J/kg × Q • **count all pixel hits** and assume average energy deposit per hit of 30 keV with 1 keV=1.6×10^{-16} J. With this method no specific quality factor can be applied and strictly one cannot come to a dose in Sv. One needs the mass of the sensor chip (0.137 g of Si) in order to normalize the energy deposition per kg. In both methods also the actual exposure time is needed to normalize the dose to μSv/h or to mSv/year.

These methods, while 'naive' approximations, produce already fairly coherent results. A cluster consisting of 10 pixels would have energy deposit of 300 keV which corresponds to 3.5×10^{-10} Sv, not far from the calibrated average value of 2×10^{-10} Sv. Measuring the actual energy deposition in each pixel, as can be done in the Timepix detector, more precise measurements can be performed as shown in Section 6.

4. Radiation measurements in ATLAS at the LHC

Because of the extreme sensitivity of the quantum imaging dosimetry and its capability to distinguish the components of the radiation environment, it appeared that measurements with Medipix2 could provide early information on the actual radiation inside the ATLAS detector at the CERN Large Hadron Collider LHC. These measurements could then be used to benchmark the original radiation simulations. 14 specially modified Medipix2 Si assemblies were installed in ATLAS, already in the year 2008 and later another two. This allowed to establish the background levels before operation. The system has made continuous measurements until now, during collision runs as well as during the accelerator stops in between. An important component of the radiation in ATLAS are the neutrons and it would be useful to know their intensity and approximate energy spectrum. For these neutron measurements, the sensors have been covered with layers of different neutron converter materials, as illustrated in Fig. 4a. The efficiencies of the different converter layers, i.e. the number of recorded clusters under each separate converter area divided by the known incident flux of neutrons of different energies, have been determined for all detector assemblies [10]. For example, the lithium fluoride layer is very effective in converting thermal neutrons, as can be seen in the exposure to 2.5×10^6 neutrons in Fig. 4b. For this layer the calibrated conversion efficiency is close to 1% for all assemblies [10].

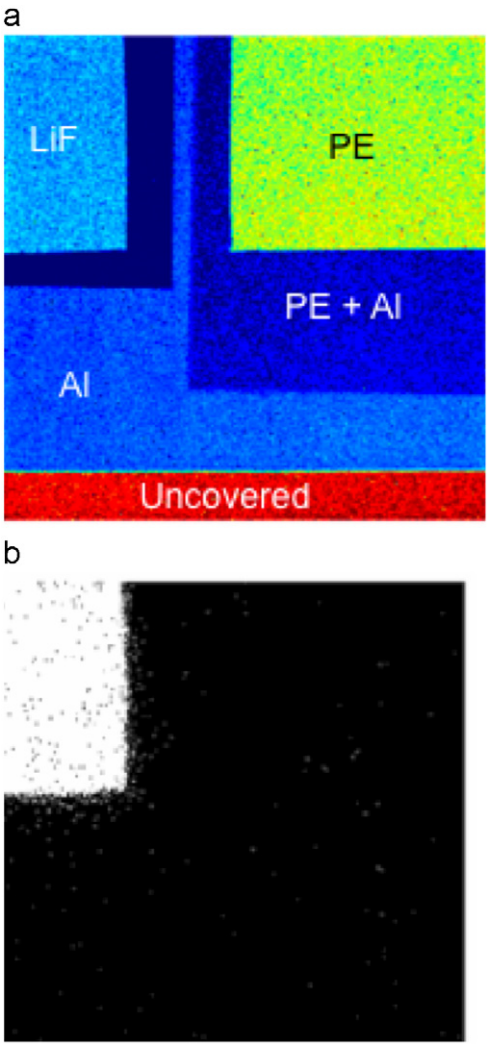

Fig. 4. (a) Layout of 3 slabs of neutron converter material, superimposed on a Medipix2 chip. A few mm remain uncovered at the bottom. (b) Frame of 500 s exposure taken in an environment of thermal neutrons with a Medipix2 chip equipped with the neutron converters of (a).

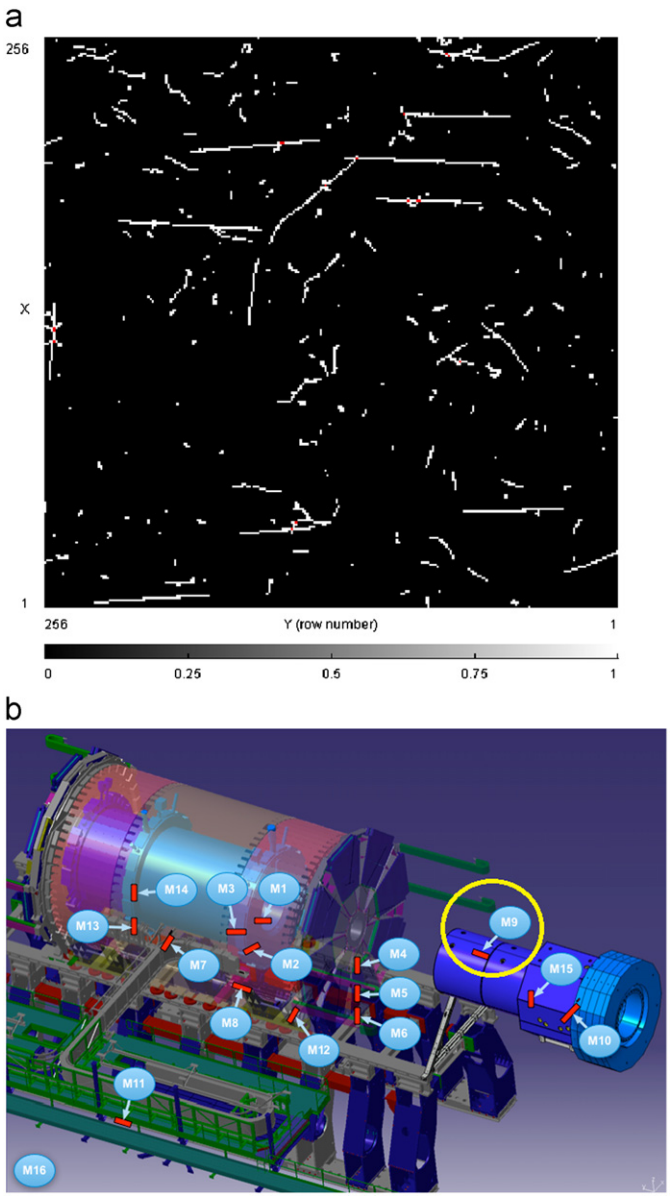

Fig. 5. (a) A 10 s exposure frame of ATLAS-MPX-09 placed behind the forward muon wheel. The ionizing trails from particles point back to the central vertex region. The cluster density here is rather too high for automatic pattern recognition. (b) Schematic view of the ATLAS detector. The ATLAS-MPX measurement stations are indicated with the small numbered blue shields. The circle indicates the one that recorded the frame of (a). (For interpretation of the references to color in this figure legend, the reader is referred to the web version of this article.)

With the relatively small neutron conversion efficiencies and the small sensor area of only $\sim 2\ \mathrm{cm}^2$, a fairly long exposure time and a large number of frames is needed in order to obtain good statistics on the neutron components. For the determination of the intensities of the ionizing particles such as electrons, muons and protons, even a small number of exposures already supplies quite precise information. A typical frame is shown in Fig. 5a. This frame is a 10 s exposure of ATLAS-MPX station 9 during a collision period. The recording includes a number of energetic particles that produce trails, pointing straight back to the interaction region. The position of this sensor in ATLAS is indicated with a circle in the diagram in Fig. 5b.

Similar frames are recorded continuously by all 16 ATLAS-MPX stations, and written on file for analysis. The evolution in time of the overall radiation can be followed and different components constantly measured in these positions. An example over a period of several days is shown in Fig. 6. One can see a decay of intensity with time during collisions, due to the proton losses in both beams. Immediately after the beams are switched off, the radiation level is still higher than after some hours. This allows study of the characteristics of local activation in surrounding material. In this background radiation one does not observe the heavy ionization clusters that occur during collision periods (purple and rose colored in the diagram). An extensive report on the first results of the ATLAS-MPX system is forthcoming [11].

5. Comparison of in-flight and sea level measurements.

With the small size of a Medipix imager and USB readout, it is easy to make measurements in an airplane. A typical example is shown in Fig. 7a, which is a frame taken at 10 km altitude, with a 60 s exposure time. The imager plane was held vertical (sometimes called 'longitudinal' or 'parallel' exposure), and apparently the muons make fairly long trails perpendicular to the surface of the earth, so that muon-like trails can be distinguished from the electron-like trails. No neutron conversion layers are present on the device used here. A dose rate of 1.7 μSv/h can be deduced from this measurement. The cluster counting method is used as explained in Section 3, except for the identified, long muon trails where the number of pixels is counted. A frame taken under exactly identical conditions at the SLAC laboratory, close to sea level, is shown for comparison in Fig. 7b and the dose rate here is only 0.1 μSv/h.

Sea level cosmic radiation and its effect on silicon microelectronics has been discussed at some length, among others, by Ziegler [12,13]. At sea level it mostly consists of neutrons and these can have various effects. However, these neutrons are not easy to measure, and with an imaging detector such as Medipix one sees mostly electrons and occasional muons. The proportion of energetic muons is much higher at flight altitude, and with this simple detector it would be possible to study the altitude dependence in detail. There is work going on in this direction [14].

In the following set of frames in Fig. 8a and b the angular dependence is shown at flight altitude. At the left the exposure was 'longitudinal' as in Fig. 7a, while the frame at the right was taken with the imager flat compared to the earth surface (confusingly called 'perpendicular'). The overall number of clusters is slightly higher (119 vs 99). This is related to the difference in area ($14\ \mathrm{mm} \times 14\ \mathrm{mm}$ vs $14\ \mathrm{mm} \times 0.3\ \mathrm{mm}$) exposed to the perpendicular atmospheric component. It is still possible to assign a muon signature to some of these clusters, but the actual length of muon clusters is much smaller. Eventually it would be feasible to determine an approximate angular distribution for the higher momentum particles, using the entrance and exit points of their trails in the well-defined 3-D sensor structure.

One also might determine the total number of hit pixels as a measure of the dose, but this number would even be more dependent on the exposure angle that is used. It is likely that cluster counting should result in a more reliable dose measurement.

Another observation in Fig. 8b is the heavy trail in the left lower corner ($x=240$, $y=10$). Such a heavy trail most likely is a low energy proton. A quality factor of 20 has been assigned to this cluster, which adds to the already higher equivalent dose in this 'perpendicular' exposure. Also nuclear fragments such as ionized Fe atoms might be recognized. Those usually appear as a small cone of hit pixels.

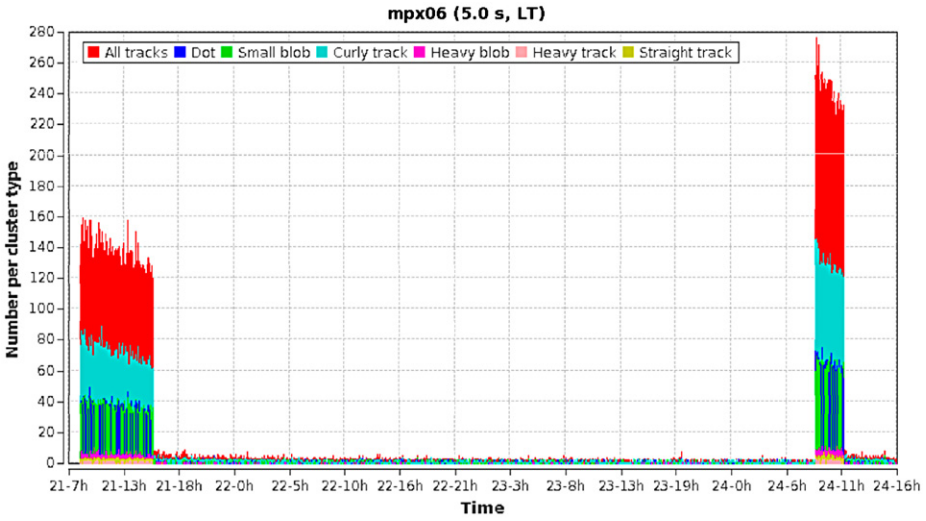

Fig. 6. Evolution in time of the radiation measured in ATLAS-MPX-06. The different types of clusters (see Fig. 2) are indicated by different colors, while red gives the sum of all clusters in each timeframe. (For interpretation of the references to color in this figure legend, the reader is referred to the web version of this article.)

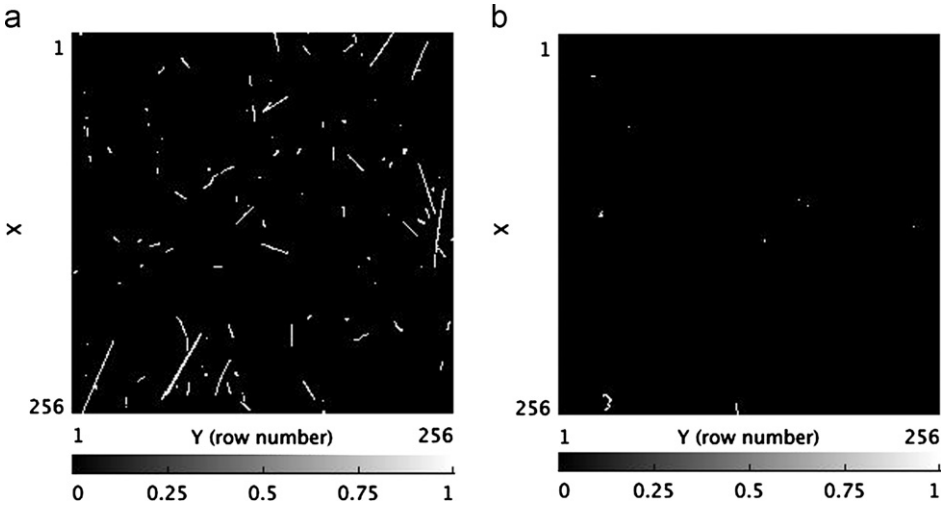

Fig. 7. (a) 60 s exposure at 10 km altitude. 105 clusters of which 36 muons. Dose rate 0.9+0.8 μSv/h (electrons, resp. muons). (b) 60 s exposure at SLAC, ~sea level 9 clusters. Dose rate 0.1 μSv/h.

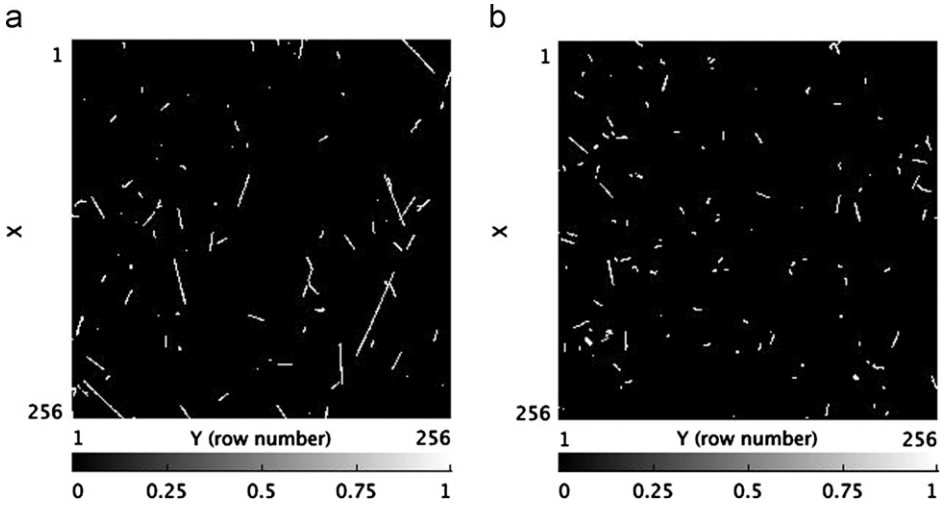

Fig. 8. (a) 60 s exposure, at 10 km altitude 99 clusters, of which 35 muons. Dose rate 1.5 μSv/h. (b). 60 s 'perpendicular' exposure at10 km, imager is kept parallel to earth surface/flight plane; 119 clusters, 31 muons. Much shorter muons, 1 heavy trail. Dose rate 1.8 μSv/h.

6. Natural background and anomalous airborne alpha particles

The quantum imaging dosimetry system with a Medipix2 or Timepix assembly is compact and can be controlled from a laptop or PC, using the software 'Pixelman' [15]. The photograph in Fig. 9 shows the full system as it can be deployed practically anywhere, using the small size USB readout [5] (Fig. 1) or the recent, even smaller 'USB Lite' [16].

Measurements have been made using the Timepix imager for characterization of the natural radiation environment in various places. While the pixels have the same analog signal processing and 14-bit register, this imager differs from the Medipix2 assembly used in the previous sections, mostly in that it has a clock distributed to each pixel, which can be used to perform local timing operations [8]. The amplitude of an analog signal from incident radiation can be digitized in each pixel by counting the clock pulses during the Time-over-Threshold. This TOT counting is fairly linear over a range of signals, as is illustrated in Fig. 10 with the response curve of one pixel.

An example of a fairly long, nearly 60 min exposure made somewhere in the countryside is shown in Fig. 11a. A color code represents the energy values that have been recorded in the pixels. In this image 650 clusters have been recorded, including 3 alpha particle impacts and 1 very long high energy electron trail. The simple method using 646 'normal' clusters, respectively 4 special ones ($Q=20$ resp 18) results in an approximate equivalent dose rate of 0.13 μSv/h, respectively 0.02 μSv/h, with sum 0.15 μSv/h. Using the TOT mechanism one can have more precise information on the deposited energy in each pixel. With a common calibration for all pixels, following the typical response curve in Fig. 10, the overall energy deposition of the 646 clusters in 3417 pixels amounts to 63 MeV. The 4 special clusters deposit ~11 MeV (3 MeV for each alpha and 2 MeV for the long trail). In a simplified approach, taking $Q=20$ for the three alpha impacts, this results in a dose rate of 0.07 μSv/h, respectively 0.2 μSv/h, with a sum nearly twice as high of 0.27 μSv/h. It appears clearly that the alpha impacts acquire a lot of weight, while apparently electromagnetic clusters contribute less than in the simple cluster method. The dose rates end up the same within a factor of two. Large fluctuations result from the low statistics of alpha particle impacts on the small detector area and the use of the quality factor. The assignment of somewhat arbitrary quality factors to such single clusters seems out of place and has to be studied for

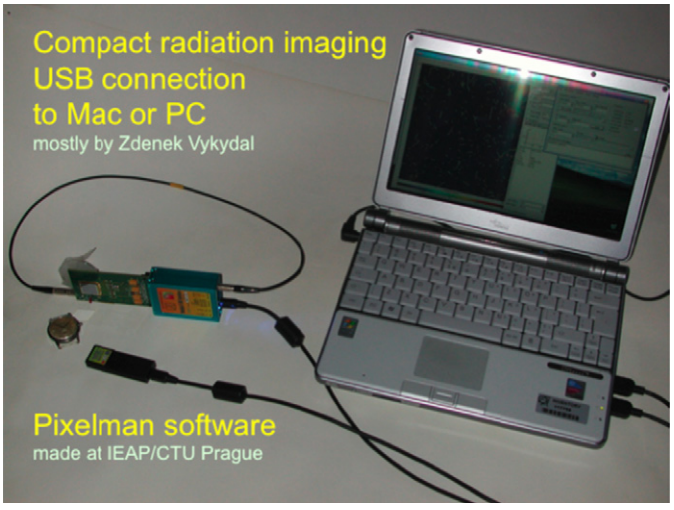

Fig. 9. Laptop with two Medipix USB devices connected and an old watch for testing that contains radium on the dial.

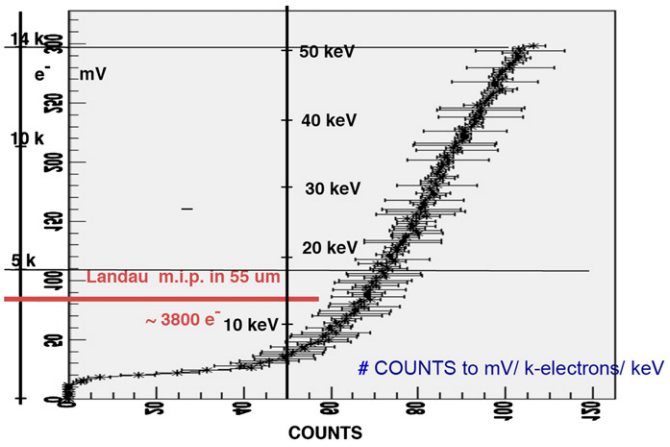

Fig. 10. Measurement of the response of the TOT mechanism in one pixel. A mV signal (here the vertical axis) is injected via the test capacitor, and the resulting number of counts was recorded. Here the curve is literally mirrored in order to make it easier to evaluate the radiation measurements in practice, where a number of counts has to be converted to a charge (in thousands of electrons) or energy deposition (keV) signal. The typical signal of 3800 e^- is generated when a particle crosses a 55 μm pixel sideways.

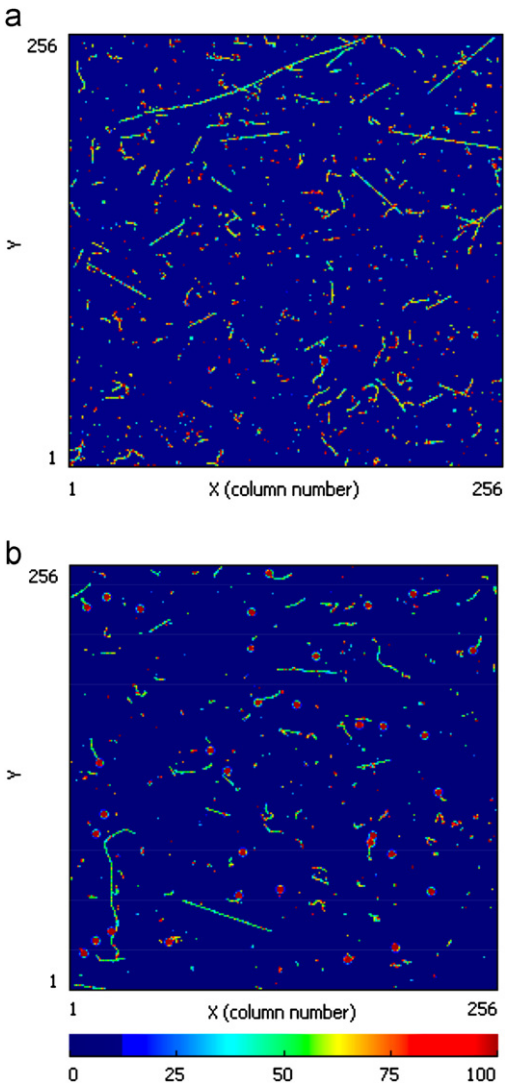

Fig. 11. (a) Frame recorded using Timepix. Exposure time 3560 s The dose rate is discussed in the text: between 0.15–0.27 μSv/h. (b) Frame as in (a), exposure 1400 s 244 clusters of which 34 alpha from decays. The dose rate is 6.8 μSv/h.

this new method of quantum imaging dosimetry. In any case, a better insight in the actual radiation environment is provided.

An unexpected illustration of the usefulness of alpha impact pattern recognition was obtained by chance on 23 June 2010, when a relatively large number of airborne alpha particles fortuitously was recorded. Fig. 11b shows one of the frames taken at that moment. Normally during a 30 min exposure only very few alpha incidences are recorded, or most often none at all. Now there were 34 during this 23 min exposure and this rate persisted during several hours. For the energy deposition by these alpha particles some assumptions have again to be made, as the sensor and associated readout are not linear, nor well calibrated in this regime. Assuming again 3 MeV per particle cluster, and applying the admittedly arbitrary quality factor $Q=20$, the dose rate for this alpha component largely exceeds that of the other components, with 6.7 μSv/h. Actually, given that these alpha particles are well recognized and airborne, and easily inhaled, a much higher quality factor might be justified. The electromagnetic component in this image, 210 clusters with energy deposit of 22 MeV represents a dose rate of 0.07 μSv/h, quite similar to that in the frame of Fig. 11a. Normalized, the total recorded dose corresponds to at least 5.9 mSv/year, but of course was only present during a limited time. The maximum permissible dose, averaged over 5 years, for radiation workers should not exceed 20 mSv/year [17]. The anomalous alpha intensity may have been related to unusual release of contaminants, in particular polonium, in industrial smoke from a nearby phosphorus fertilizer plant.

7. Conclusion

With the Medipix family of radiation imaging detectors one can measure dose and dose rate over a dynamic range of $>10^{14}$ with a single device, starting from extremely low intensities, far below dangerous levels. The radiation is sampled by the $\sim 2\ \mathrm{cm}^2$ sensor with accurately adjustable exposure times. The 0.3 mm thick silicon sensor has at least some sensitivity to X-ray photons and neutrons. Sensitivity for these neutral particles could be improved by using thicker silicon or a different semiconductor sensor. Also, converters are helpful in some cases. Quality factors can be assigned to different classes of radiation quanta, because these can be characterized by pattern recognition in the imager. Some examples have been discussed and the measurements already agree fairly well with dose obtained by classical means. More work is needed to exploit the full potential of this method of quantum imaging dosimetry and to achieve precise determination of equivalent dose. The small-size system can be used in nearly all circumstances, and it is controlled with a portable computer. Such systems could play a role in physics education and may contribute to more widespread and better understanding of the natural radiation environment.

Acknowledgments

This work has been performed in the framework of the Medipix2 collaboration (〈http://medipix.web.cern.ch/MEDIPIX/〉) which has funded the development and manufacturing of the detector assemblies. The USB readout modules have been developed and produced at the Institute of Experimental and Applied Physics IEAP of the Czech Technical University in Prague.

References

[1] E.H.M. Heijne, Nuclear Instruments and Methods A465 (2001) 1. (Genova, Pixel Workshop—2000).
[2] Andrey Starodumov, Roland Horisberger, Danek Kotlinski, Recent reports have been presented on the ALICE Silicon Pixel Detector, the ATLAS Pixel, the CMS Pixel and on the LHCb–RICH readout which uses pixel chips in a phototube, in: Proceedings of the International Workshop on Semiconductor Pixel Detectors for Particles and Imaging, 2010, Nuclear Instruments and Methods A 659 (2011) pp. 1–256.
[3] T. Holy, E. Heijne, J. Jakubek, S. Pospisil, J. Uher, Z. Vykydal, Nuclear Instruments and Methods A 591 (2008) 287.
[4] J. Bouchami, A. Gutierrez, T. Holy, A. Houdayer, J. Jakubek, C. Lebel, C. Leroy, J. Macana, J.-P. Martin, S. Pospısil, S. Prak, P. Sabella, C. Teyssier, Nuclear Instruments and Methods A 633 (2011) S187.
[5] Zdenek Vykydal, Jan Jakubek, Stanislav Pospisil, Nuclear Instruments and Methods A 581 (2006) 112.
[6] X. Llopart, M. Campbell, D. San Segundo, E. Pernigotti, R. Dinapoli, IEEE Transactions on Nuclear Sciences NS-49 (2002) 2279.
[7] M. Campbell, E.H.M. Heijne, G. Meddeler, E. Pernigotti, W. Snoeys, IEEE Transactions on Nuclear Science NS-45 (1998) 751.
[8] X. Llopart, R. Ballabriga, M. Campbell, L. Tlustos, W. Wong, Nuclear Instruments and Methods A581 (2007) 485.
[9] R. Ballabriga, M. Campbell, E.H.M. Heijne, X. Llopart, L. Tlustos, IEEE Transactions on Nuclear Science NS-54 (2007) 1824.
[10] D. Greiffenberg, M. Fiederle, Z. Vykydal, V. Král, J. Jakůbek, T. Holý, S. Pospíšil, D. Maneuski, V. O'Shea, M. Suk, M. Králík, C. Lebel, C. Leroy, Nuclear Instruments and Methods A 607 (2009) 38.
[11] ATLAS-MPX Report, in preparation.
[12] J.F. Ziegler, W.A. Lanford, Science 206 (1979) 206.
[13] J.F. Ziegler, H.W. Curtis, H.P. Muhlfeld, C.J. Montrose, B. Chin, M. Nicewicz, C.A. Russel, W.Y. Wang, L.B. Freeman, P. Hosier, L.E. LaFave, J.L. Walsh, J.M. Orro, G.J. Unger, J.M. Ross, T.J. O'Gorman, B. Messina, T.D. Sullivan, A.J. Sykes, H. Yourke, T.A. Enger, V. Tolat, T.S. Scott, A.H. Taber, R.J. Sussman, W.A. Klein, C.W. Wahaus, IBM Journal of Research and Development 40 (1996) 3.
[14] J. Urbar, J. Scheirich, J. Jakubek, Nuclear Instruments and Methods A 633 (2011) S206.
[15] D. Turecek, T. Holy, J. Jakubek, S. Pospisil, Z. Vykydal, Pixelman: a multiplatform data acquisition and processing software package for Medipix2, Timepix and Medipix3 detectors, in: Proceedings of the 12th IWoRID, Cambridge, 2010, JINST 6 C01046, 10.1088/1748-0221/6/01/C01046.
[16] Z. Vykydal, J. Jakubek, Nuclear Instruments and Methods A 633 (2011) S48, http://dx.doi.org/10.1016/j.nima.2010.06.118.
[17] See for example 〈http://www.world-nuclear.org/education/ral.htm〉.